

Article

# An Automated Mapping Method of 3D Geological Cross-Sections Using 2D Geological Cross-Sections and a DEM

Hao Shang <sup>1</sup>, Yan-Gen Shen <sup>2</sup>, Shuang Li <sup>1</sup>, An-Bo Li <sup>2,3,4,\*</sup>  and Tao Zhang <sup>1</sup>

<sup>1</sup> Shandong Institute of Geological Survey, Jinan 250014, China

<sup>2</sup> Key Laboratory of Virtual Geographic Environment, Ministry of Education, Nanjing Normal University, Nanjing 210023, China

<sup>3</sup> Jiangsu Center for Collaborative Innovation in Geographical Information Resource Development and Application, Nanjing 210023, China

<sup>4</sup> State Key Laboratory Cultivation Base of Geographical Environment Evolution (Jiangsu Province), Nanjing 210023, China

\* Correspondence: mrlab@njnu.edu.cn; Tel.: +86-136-4516-1205

**Abstract:** With the three-dimensional (3D) geological information system development, 3D geological cross-sections (GCs) have become the primary data for geological work and scientific research. Throughout past geological surveys or research works, a lot of two-dimensional (2D) geological cross-section maps have been accumulated, which struggle to meet the scientific research and application needs of 3D visual expression, 3D geological analysis, and many other aspects. Therefore, this paper proposes an automatic generation method for 3D GCs by increasing the dimensions based on a digital elevation model (DEM) and 2D geological cross-section maps. By matching corresponding nodes, generating topographic feature lines, constructing an affine transformation matrix, and inferring the elevation value of each geometric node on the GC, the 3D transformation of the 2D GCs is realized. In this study, fourteen 2D GCs within Nanjing City, Jiangsu Province, are transformed into 3D GCs using the proposed method. The transformed results and quantitative error show that: (1) the proposed method applies to both straight and bent GCs; (2) each transformed GC can fit seamlessly with the ground and maintain minimal geometric deformation, and the geometric shape is consistent with the original GC in non-mountains area. This paper corroborated the proposed method's effectiveness by comparing it with the other two 3D transformation strategies. In addition, the transformed GCs can be subjected to 3D geological modeling and digital Earth presentation, achieving positive effects in both 3D application and representation.

**Keywords:** geological cross-sections; 3D presentation; DEM; spatial transformation; 3D modelling



**Citation:** Shang, H.; Shen, Y.-G.; Li, S.; Li, A.-B.; Zhang, T. An Automated Mapping Method of 3D Geological Cross-Sections Using 2D Geological Cross-Sections and a DEM. *ISPRS Int. J. Geo-Inf.* **2023**, *12*, 147. <https://doi.org/10.3390/ijgi12040147>

Academic Editors: Sisi Zlatanova and Wolfgang Kainz

Received: 1 February 2023

Revised: 19 March 2023

Accepted: 27 March 2023

Published: 29 March 2023



**Copyright:** © 2023 by the authors. Licensee MDPI, Basel, Switzerland. This article is an open access article distributed under the terms and conditions of the Creative Commons Attribution (CC BY) license (<https://creativecommons.org/licenses/by/4.0/>).

## 1. Introduction

The geological cross-section (GC) is a map reflecting the strata and geological structures at a certain depth on the ground and underground in a specific direction and is the primary datum for studying the stratum, rock mass, and geological structures [1]. A single GC depicts the configuration of many rock units as typically viewed in a vertical plane, which can clearly define the spatial distribution of rock strata, the development of geological structures, and specific geological relations [2,3], and it is a vital data source in geological field surveys [4], petroleum exploration [5], underground engineering [6], etc. In addition, the GCs, in association with the planar geological maps, enable a 3D concept of the geological structures [7,8], reflecting the spatial interrelationship between the geological bodies and the geological structures [9] as well as the evolution of geological relationships [10]. Geologists have long produced and accumulated numerous GC maps based on the significance of GCs in research and application.

There are many types of GCs with various classification methods [11]. According to the angle with the structural strike, they can be divided into a dip GC (oriented perpendicular

to the strike of the structure), a strike GC (oriented parallel to the strike of the structure), and an oblique GC (oriented obliquely to the structural axis) [8]. According to different expression contents, they can be divided into a stratigraphic GC, structural GC, intrusive rock GC, Quaternary GC, volcanic rock GC, etc. According to different mapping methods, they can be divided into a surveyed GC and a transverse cutting GC [12]. The above different GCs have brought great help to geological work [4–10]. The 2D GCs studied in this paper must express the stratigraphic information perpendicular to the ground surface and have a vertical Y-axis. Such GCs are also the most common in the geological field.

Many geological studies or investigations have exhibited GCs as 2D maps for a long time. On the one hand, due to the convenient preservation and transmission of 2D geological maps, many scholars or geological survey departments will directly obtain the 2D GCs through field surveys [13], borehole stratigraphic correlation mapping [14–16], transverse cutting GC deduction [7,17], and deep learning [18]. On the other hand, restricted by early mapping technology, the 2D geological maps are the primary means to retain geological information in the absence of the development of 3D electronic maps. Therefore, a series of early 2D geological maps have been saved [19]. These geological maps and the attached GCs provide strong evidence for studying the stratigraphic distribution and geological structure development in the historical period. Compared with the 2D GC, the 3D GC can more intuitively express the development condition of underground strata [1,12], so it has more essential research significance and application value in the era of the 3D Geographic Information System (GIS). For one thing, to better exhibit the rock strata's geometric shape and contact relationship in the 3D model of the geological body, it is often necessary to build 3D GCs in the form of a coulisse diagram [1], fence diagram [12,20], or block diagram [8,20]. For another, the 3D GCs have always been a vital data source for the 3D modeling of geological bodies [21–25]. Relevant modeling algorithms are also becoming mature, such as the 3D geological body modeling methods based on 2D or 3D GCs [7,22,23], multi-source data [21,25], contour lines [26–28], morphing algorithm [29], discrete smooth interpolation (DSI) algorithm [30], etc.

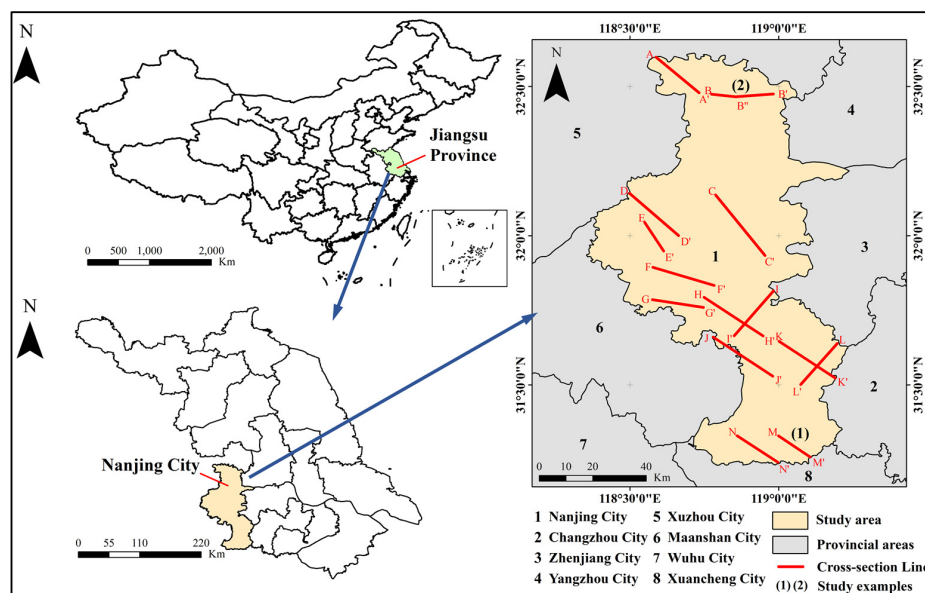
In general, with the constant maturity of 3D GIS technology and the increasing expansion of 3D geoscience application systems, the traditional 2D GCs struggle to meet the user's scientific research and application needs in 3D visual expression, 3D spatial analysis, and many other aspects. Therefore, taking the 2D geological cross-section line (GCL) and a DEM as the basic data to control the spatial geometry and ground elevation of the GC, and taking the stratum surface in the GC as the study unit, this paper proposed an automatic generation method of the 3D GC by increasing dimensions of the 2D GC. Specifically, this work was structured as follows: Section 2 describes the study area and input data; Section 3 describes the methodology; Section 4 describes the transformed results; Section 5 describes the discussion and applications; and Section 6 describes the conclusion.

The content studied in this paper has several practical and geological significance, as follows: (1) Based on ensuring minimum geometric deformation, the automatic 3D transformation of 2D GCs attached to planar geological maps is performed. (2) Displaying planar geological maps and GCs simultaneously in a 3D scene provides an intuitive 3D visualization of geological structures, which is more conducive to recognizing and transmitting geological information. (3) If there are two parallel and adjacent 2D GCs in a local area, after 3D transformation, a 3D geological model can be constructed using a 3D modeling method based on parallel GCs. Alternatively, one or two similar parallel GCs can be generated within a certain strip distance on one or two sides of a 3D transformed GC. These GCs can be used to construct a local 3D geological solid based on the 3D modeling method mentioned above. (4) The surface relief of 2D GCs mapped during historical periods may not be consistent with the current terrain. It is necessary to constrain 3D transformation through the current DEM to conform to the current geometric form.

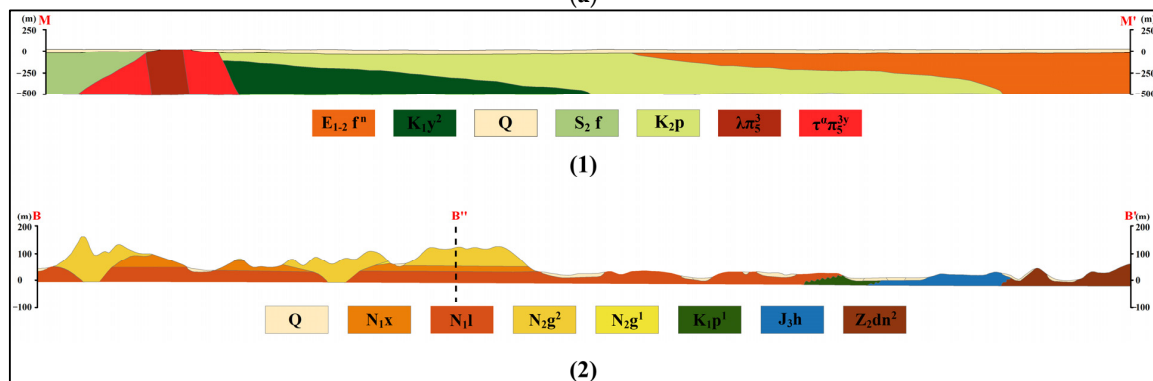
## 2. Study Area and Input Data

### 2.1. Study Area

The study area is part of the Nanjing-Zhenjiang mountains, located in Nanjing City, Jiangsu Province, China, ranging from 118°20' E to 119°14' E, 31°13' N to 32°33' N (Figure 1a). The area is well developed from Sinian to Quaternary, and Quaternary strata (Q) and bedrock are distributed alternately [31]. The Quaternary strata cover a wide area and are shallow, while the bedrock is scattered in blocks. The study area is suitable for geological investigation and research because of its well-developed strata, various magmatic rocks, and typical geological structure including folds, faults, and intrusion tectonics. During 1970–1990, the Jiangsu Provincial Bureau of Geology and Mineral Resources conducted a geological field survey on the Nanjing-Zhenjiang Mountains and mapped a series of 1:50,000 2D geological maps. Fourteen GCs and corresponding GCLs were generated within Nanjing City (Figure 1a), including thirteen straight GCs (Figure 1b(1) shows an example for GC M-M') and one bent GC (Figure 1b(2) for B-B''-B'). Most GCs in the study area show the NW–SE trend, while GCs I-I' and L-L' show the NE–WS trend, and GC B-B''-B' shows a W–E trend. Currently, all GCs and GCLs are 2D. In this study, fourteen GCs in the study area will be transformed into 3D GCs, and 3D solid models of all geological bodies will be constructed locally.



(a)



(b)

**Figure 1.** (a) The location of the study area and the distribution of GCLs. (b) Schematic diagram of two typical GCs. The GC M-M' is straight, and the GC B-B''-B' is bent.

## 2.2. Input Data

The input data include the DEM, 2D vector GCs, and 2D GCLs, where the DEM (ESRI (Environmental Systems Research Institute) grid format) is derived from the Geospatial Data Cloud (<http://www.gscloud.cn/>) (Released data in 2009, Version 1, and accessed on 6 August 2022), which belongs to ASTER GDEM data product, and the spatial resolution is 30 m. This DEM is currently a publicly released product with the highest precision, the broadest coverage, and is easy to obtain. The GCs are vector polygon data, and the GCLs are vector polyline data, both in ESRI Shapefile format and a GC corresponds to a GCL. The GCs are located in Cartesian coordinates. The geographic coordinate system of the GCLs and DEM is WGS84, and the map projection is Universal Transverse Mercator (UTM). All GCs were mapped by the Jiangsu Provincial Bureau of Geology and Mineral Resources during 1970s–1990s.

## 3. Methodology

The proposed method in this study takes the stratum surface in the GC as the experimental unit, mainly including the following four processing steps: (1) matching the corresponding nodes between the GC and the GCL and generating the internal feature lines; (2) calculating affine transformation parameters and constructing affine transformation matrix; (3) calculating the node  $z$  value to obtain the 3D stratum surface based on the ground elevation and the position of each node on the stratum polygon; (4) merging all 3D strata surfaces to obtain a 3D GC. If the GCL is bent, it is necessary to divide the GC at the turning point vertically, then to use steps (1)–(4) to process each divided GC, and finally to merge all the divided parts. Figure 2 shows the flow chart for generating 3D GCs based on 2D GCs by increasing dimensions. The following will take GCs M-M' (Figure 1b(1)) and B-B''-B' (Figure 1b(2)) as the actual cases of straight GC and bent GC, respectively, and detail the proposed method.

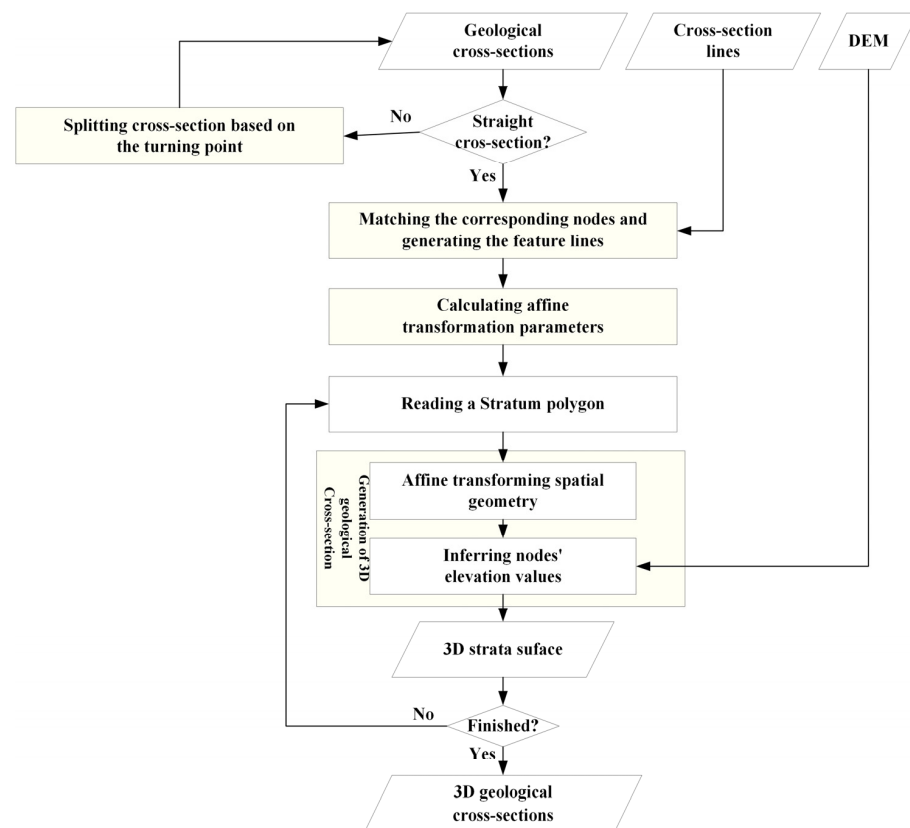


**Figure 2.** Flow chart of generating 3D GCs based on 2D GCs by increasing dimensions.

### 3.1. Matching the Corresponding Nodes and Generating Feature Lines

The 2D GC is usually formed by the projection transformation of the 3D geological information and mapping it onto the map, and its 2D spatial coordinates, direction, and scale are changed, which is inconsistent with the actual GC geometry [8]. Thus, it is necessary to adjust its spatial geometry on the XY plane prior to constructing a 3D GC. The affine transformation [32–34] enables the geometric topology, scale, or spatial relationships of an image or geometry to be consistent before and after the transformation. In order to maintain the consistency of the above spatial features in the 2D GCs in this study before and after transformation, the affine transformation is the best choice. The affine transformation mainly includes two core steps: matching corresponding points; and calculating affine transformation parameters including translation length, rotation angle, scaling coefficient, etc., and the former is the basis of the latter. In this study, we will find or create two nodes from the 2D GC to correspond with the starting node and the ending node of the straight GCL and further calculate the affine transformation parameters.

The boundary lines on the left and right sides of the 2D GC provided in this study are strictly perpendicular to the X-axis in the planar coordinate system, so two nodes (nodes  $P_l$  and  $P_r$  in Figure 3), corresponding with the starting node and the ending node of the straight GCL, can be obtained on both sides by constructing a line (transform line, TL, in Figure 3) perpendicular to the two vertical boundary lines. In addition, the top line between (ground line, GL, in Figure 3) two nodes (nodes  $P_l$  and  $P_v$  in Figure 3) in the upper left corner and the upper right corner of the 2D GC represents the surface undulation. In Section 3.3, it can help to judge whether the nodes are located on the surface, so it needs to be generated in advance.

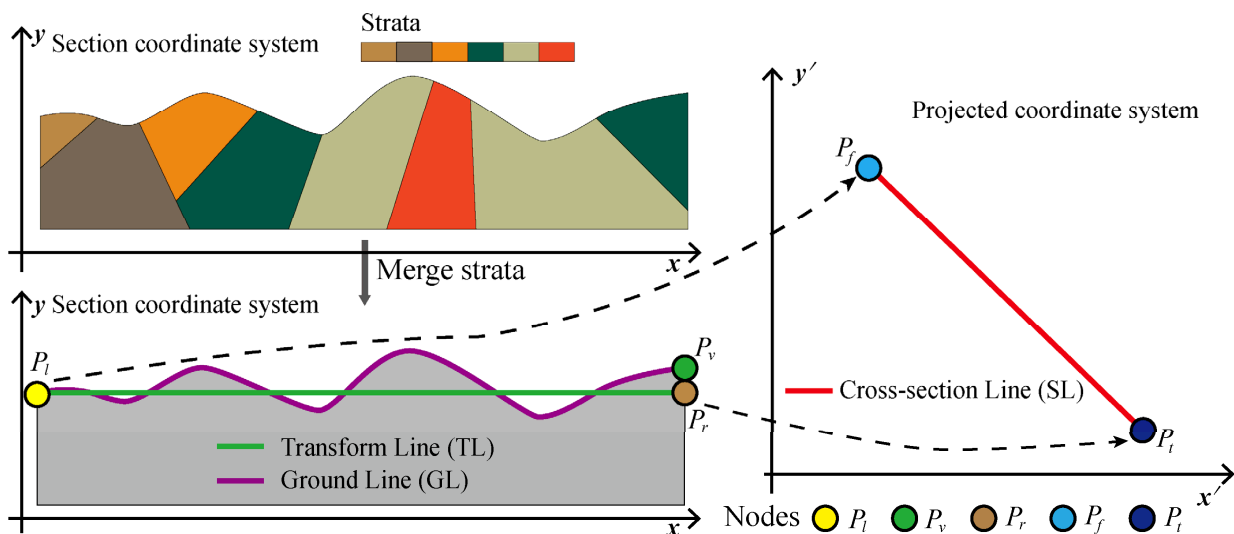


**Figure 3.** Schematic diagram of corresponding nodes matching and feature lines generation.  $x$ - $y$  and  $x'$ - $y'$  represent the GC and the GCL in different coordinate systems.

The following calculations detail how to obtain corresponding nodes and generate feature lines in the Cartesian coordinate system, and the Y-axis represents the north (Figure 3):

- (1) Loading data. Reading any 2D GC and its corresponding GCL, then saving the strata surfaces in the GC into  $S = \{s_o | o = 1, 2, \dots, ON\}$ , where  $o$  means the index of each stratum surface,  $ON$  is the number of strata surfaces and the GCL is SL, respectively;
- (2) Matching corresponding node pairs. Firstly, merging all strata surfaces in the set  $S$  to obtain a complete polygon  $P$ , then obtaining node  $P_l = (x_l, y_l)$  with the smallest X value and the largest Y value in  $P$  and node  $P_v = (x_v, y_v)$  with the largest X value and the largest Y value, respectively, creating a node  $P_r = (x_r, y_r)$  with an X value equal to  $x_v$  and a Y value equal to  $y_l$ . Finally, obtaining the starting point  $P_f = (x_f, y_f)$  and

- ending point  $P_t = (x_t, y_t)$  of the GCL and constructing corresponding node pairs with node  $P_l$  and node  $P_r$ ;
- (3) Generating feature lines. Taking  $P_l$  as the starting node and  $P_r$  as the ending node to construct a straight line, which is called the transform line, TL. Dividing the outer boundary of polygon P at nodes  $P_l$  and  $P_r$  and segmenting the boundary starting from node  $P_l$  and ending at node  $P_v$  as the ground line, GL.

### 3.2. Computing Affine Transformation Parameters and Generating Matrix

According to the corresponding node pairs matched in Section 3.1, the affine transformation parameters of the GC can be further calculated and stored in the matrix. Similarly, the following calculations are in the Cartesian coordinate system, and the Y-axis represents the north.

First, applying the nodes  $P_l = (x_l, y_l)$ ,  $P_r = (x_r, y_r)$ ,  $P_f = (x_f, y_f)$ , and  $P_t = (x_t, y_t)$  to calculate the required affine transformation parameters according to Formula (1) (Figure 4), and then constructing the affine transformation matrix AT according to Formula (2).

$$\begin{cases} \Delta x_l = 0 - x_l, \Delta y_l = 0 - y_l \\ \theta = \beta - \alpha \\ \sigma = L_{SL} / L_{RL} \\ \Delta x_t = x_t - 0, \Delta y_t = 0 - y_t \end{cases} \quad (1)$$

$$AT = \begin{bmatrix} 1 & 0 & \Delta x_l \\ 0 & 1 & \Delta y_l \\ 0 & 0 & 1 \end{bmatrix} \begin{bmatrix} \sigma & 0 & 0 \\ 0 & \sigma & 0 \\ 0 & 0 & 1 \end{bmatrix} \begin{bmatrix} \cos \theta & -\sin \theta & 0 \\ \sin \theta & \cos \theta & 0 \\ 0 & 0 & 1 \end{bmatrix} \begin{bmatrix} 1 & 0 & \Delta x_l \\ 0 & 1 & \Delta y_l \\ 0 & 0 & 1 \end{bmatrix} \quad (2)$$

where  $\alpha$  and  $\beta$  are the azimuths of line TL and line SL, respectively, solved by coordinate inverse calculation [35,36];  $L_{RL}$  and  $L_{SL}$  are the lengths of line TL and line SL, respectively, solved by the Euclidean distance equation [37];  $\Delta x_l$  and  $\Delta y_l$  are the translation distances that the node  $P_l$  moves to the origin of coordinate;  $\theta$  is the rotation angle;  $\sigma$  is the scaling coefficient;  $\Delta x_t$  and  $\Delta y_t$  are translation across which node  $P_l$  moves to node  $P_f$  again.

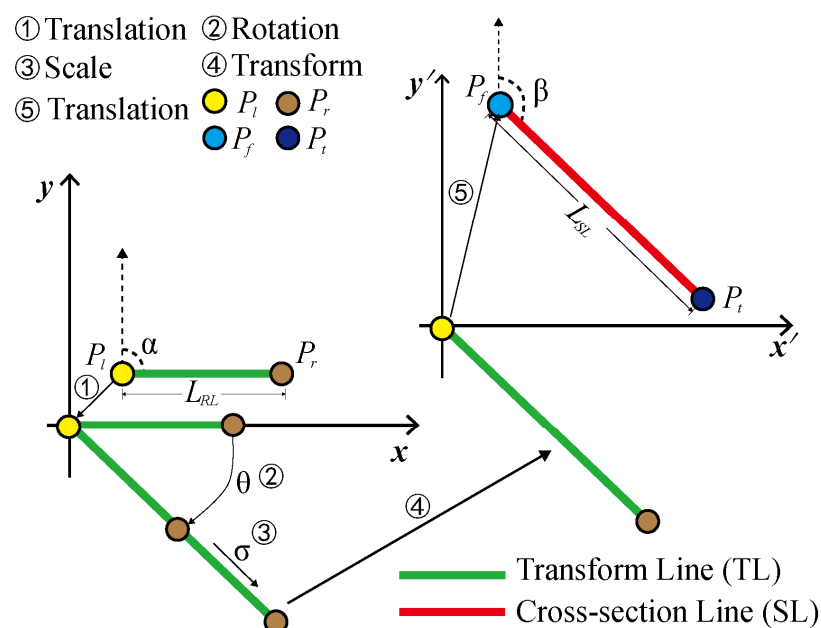


**Figure 4.** Schematic diagram of affine transformation parameter calculation.  $x$ - $y$  (the Cartesian coordinate system) and  $x'$ - $y'$  (the projection coordinate system) represent the transform line TL and the GCL SL in different coordinate systems. ①~⑤ represents the sequence of different transformation operations.

### 3.3. Generating 3D GC

First, after obtaining the affine transformation matrix AT, any node  $P_s = (x_s, y_s)$  on the stratum surface  $s_o$  can be transformed to the node  $P_s' = (x_s', y_s')$ , according to the following Formula (3), to obtain the transformed stratum surface  $s_o'$ . The above transformation processes are applied to all the strata in set S to obtain the transformed strata surfaces and save them into set  $S' = \{s_o' | o = 1, 2, \dots, ON\}$ .

$$\begin{bmatrix} x_s' \\ y_s' \\ 1 \end{bmatrix} = AT \begin{bmatrix} x_s \\ y_s \\ 1 \end{bmatrix} \quad (3)$$

where  $x_s$  and  $y_s$  are the node coordinates before the affine transformation, and  $x_s'$  and  $y_s'$  are the node coordinates after the affine transformation. AT is an affine transformation matrix.

Then, the coordinates of the stratum surface after affine transformation are still 2D, and a 3D transformation is required to meet the actual needs. Different surveying methods and strategies lead to different dip angles of GCs [8]. Due to the influence of internal and external forces on the Earth or human activities, difference of the ground elevation is apparent in different mapping times [38,39]. Given these two different situations, the GC in this study is vertical to the ground by default, and the available DEM data is used to control the stratum surface undulation.

Before and after the 3D transformation of the strata surfaces in the GC, the topology and scale relationship between the spatial geometric polygons should be consistent. This study being aimed at each node on the stratum surface has ensured the consistency of the topological relationship. Suppose the geometric proportion between the strata surfaces needs to be consistent. In this case, the distance  $d_1$  from each node to the GCL SL, the distance  $d_3$  to the line GL, and the distance  $d_2$  from the line GL to the GCL SL could be kept at an equal ratio or difference in the direction perpendicular to the GCL before and after the 3D transformation. Therefore, this study summarizes the process of 3D transformation of the stratum surface into four steps: generating intersection points, calculating distance, calculating 3D coordinates of nodes, and generating a 3D stratum surface.

- (1) Generating intersection points. Obtaining any node  $P_s' = (x_s', y_s', z_s')$  on the stratum surface  $s_o'$  boundary line to create a straight line perpendicular to the direction of the GCL SL. It intersects with the line GL and the GCL SL, respectively. The intersection points were recorded as  $P_{GL} = (x_{GL}, y_{GL})$  and  $P_{SL} = (x_{SL}, y_{SL})$ ;
- (2) Calculating distance. Calculating the Euclidean distances from node  $P_s'$  to point  $P_{SL}$ , point  $P_{GL}$  to point  $P_{SL}$ , and node  $P_s'$  to point  $P_{GL}$ , respectively, and recording them as  $d_1$ ,  $d_2$ , and  $d_3$ ;
- (3) Calculating elevation difference. The elevation values at point  $P_{SL}$  and node  $P_f'(x_f', y_f')$  (the node  $P_f$  transformed in Section 3.1) were obtained from the DEM and recorded as  $z_{SL}$  and  $z_f'$ , and the difference's absolute value  $d_4$  between them was calculated;
- (4) Calculating 3D coordinates of nodes. The node  $P_f'$  is recorded as a 3D node  $P_s'' = (x_s'', y_s'', z_s'')$  after 3D transformation. In theory,  $d_4$  and  $d_4$  are equal if the current terrain is consistent with the terrain when making the GCs. However, the terrain is dynamically changing. This study classifies different nodes according to their positions, then determines their elevation calculation equations by comparing the elevation of point  $P_{SL}$  and node  $P_f'$  and the difference between  $d_4$  and  $d_2$ . Through the experiment, it is found that all nodes are mainly distributed in four situations (Figure 5a), where  $x_s'' = x_{SL}$  and  $y_s'' = y_{SL}$ . The calculation method of the specific elevation value  $z_s''$  is shown in Table 1;
- (5) Generating a 3D stratum surface. Cycling steps (1)–(3), executing 3D transformation for all boundary nodes of stratum surface S and closing all 3D nodes to obtain a 3D stratum surface.

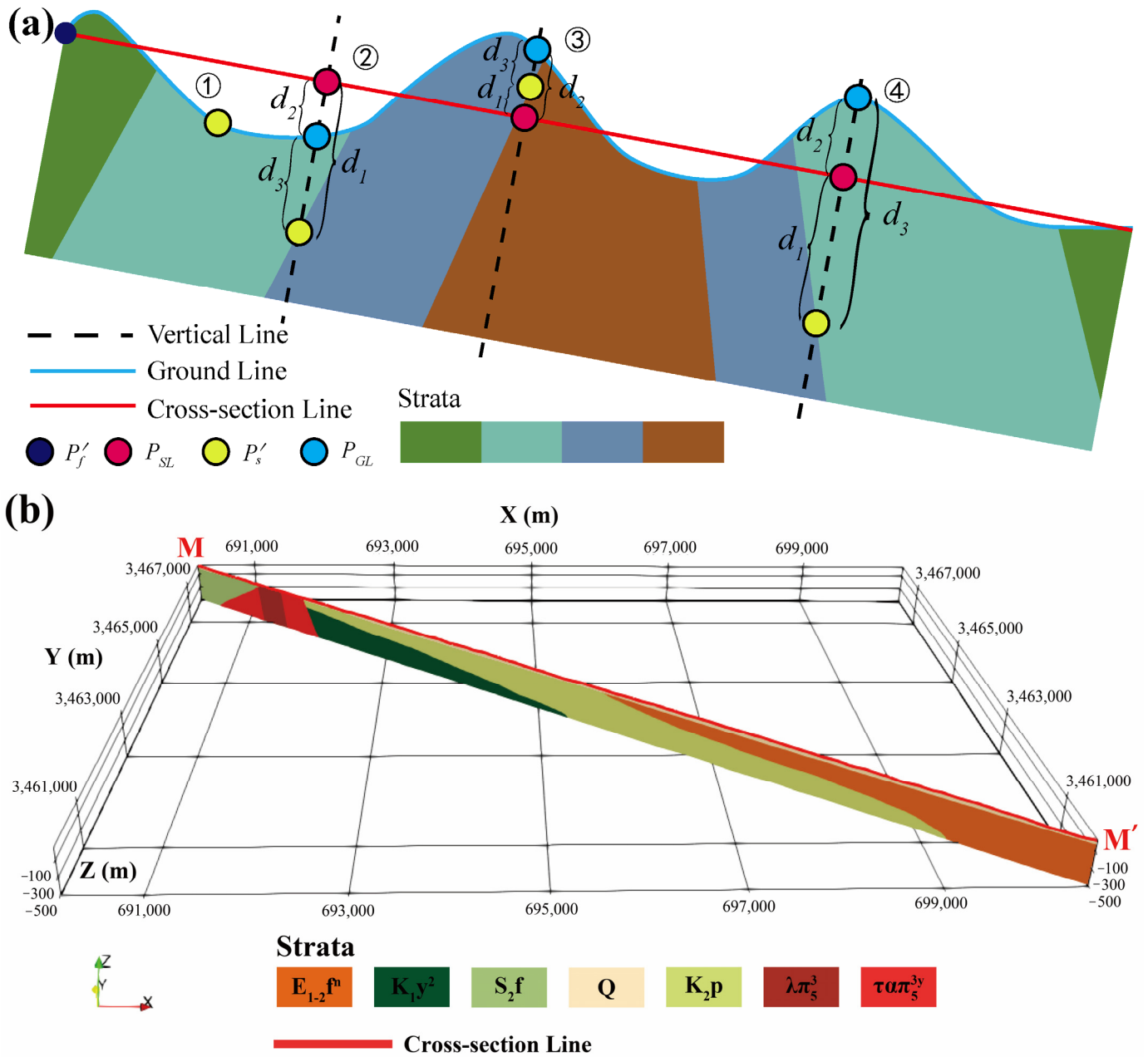


**Figure 5.** (a) Schematic diagram of different situations of nodes on the stratum surface, where the Vertical Line is perpendicular to the Section Line. (b) The 3D transformation effect of the straight GC M-M'.

**Table 1.** Elevation calculation formulas of nodes at different situations.

Type	Situation	Condition	Formula ( $z_s''$ )	Description
①	$d_2 = d_1$	-	$z_{SL}$	The node $P_s'' = (x_s'', y_s'', z_s'')$ is on the ground line.
②	$d_1 = d_2 + d_3$	$z_{f'} > z_{SL} \cap d_4 < d_2$	$z_{SL} - d_3$	The elevation at node $P_{f'}$ is still higher than the elevation at node $P_{SL}$ , and $d_4 < d_2$ .
		$z_{f'} > z_{SL} \cap d_4 > d_2$	$z_{f'} - d_1$	The elevation at node $P_{f'}$ is still higher than the elevation at node $P_{SL}$ , and $d_4 > d_2$ .
		$z_{f'} < z_{SL}$	$z_{SL} - d_3$	The elevation at node $P_{f'}$ changes to be lower than the elevation at node $P_{SL}$ .
③	$d_2 = d_1 + d_3$	$z_{f'} > z_{SL}$	$z_{SL}$	The elevation at node $P_{SL}$ changes to be lower than the elevation at node $P_{f'}$ .
		$z_{f'} < z_{SL}$	$z_{SL} - \left(\frac{d_3 \times d_4}{d_2}\right)$	The elevation at node $P_{SL}$ is still higher than the elevation at node $P_{f'}$ , but $d_4 \neq d_2$ .
④	$d_3 = d_1 + d_2$	$z_{f'} > z_{SL}$	$z_{f'} - d_1$	The elevation at node $P_{SL}$ changes to be lower than the elevation at node $P_{f'}$ .
		$z_{f'} < z_{SL} \cap d_4 > d_2$	$z_{SL} - d_3$	The elevation at node $P_{f'}$ is still lower than the elevation at node $P_{SL}$ , and $d_4 > d_2$ .
		$z_{f'} < z_{SL} \cap d_4 < d_2$	$z_{f'} - d_1$	The elevation at node $P_{f'}$ is still lower than the elevation at node $P_{SL}$ , and $d_4 < d_2$ .

Through cycling steps (1)–(4), all the strata surfaces in set  $S'$  can be transformed into 3D strata to obtain the 3D set  $S'' = \{s_o'' | o = 1, 2, \dots, ON\}$ . Then, we can obtain the 3D GC by combining all the 3D strata surfaces. Figure 5b shows the 3D GC M-M'.

### 3.4. Handling the Bent GC

In Sections 3.1–3.3, the proposed method can only deal with straight GCs and GCLs. The bent GC mapped by the bent GCL will form a straight one on the plane map after projection processing (Figure 1b(2)). Due to the GCL being bent and the mapped GC being straight, the two cannot effectively construct the corresponding points and thus cannot complete the 2D affine transformation. To improve the reusability of the above-mentioned method, this study will cut the bent GCs and GCLs. Three key steps: first, cutting the GC and GCL at the turning points to obtain multiple one-to-one straight GCs and GCLs, then transforming each branch GC into a 3D GC using the method proposed in Sections 3.1–3.3, and finally merging the cut 3D stratum surfaces. Figure 6 shows the processed results of GC B-B''-B'. Figure 6a shows the result of the affine transformation of the two-branch GCs from the GC B-B''-B' divided into two parts at the turning point B''. Figure 6b shows the merged result after 3D transformation of the two branch GCs with the 3D coordinate axis.

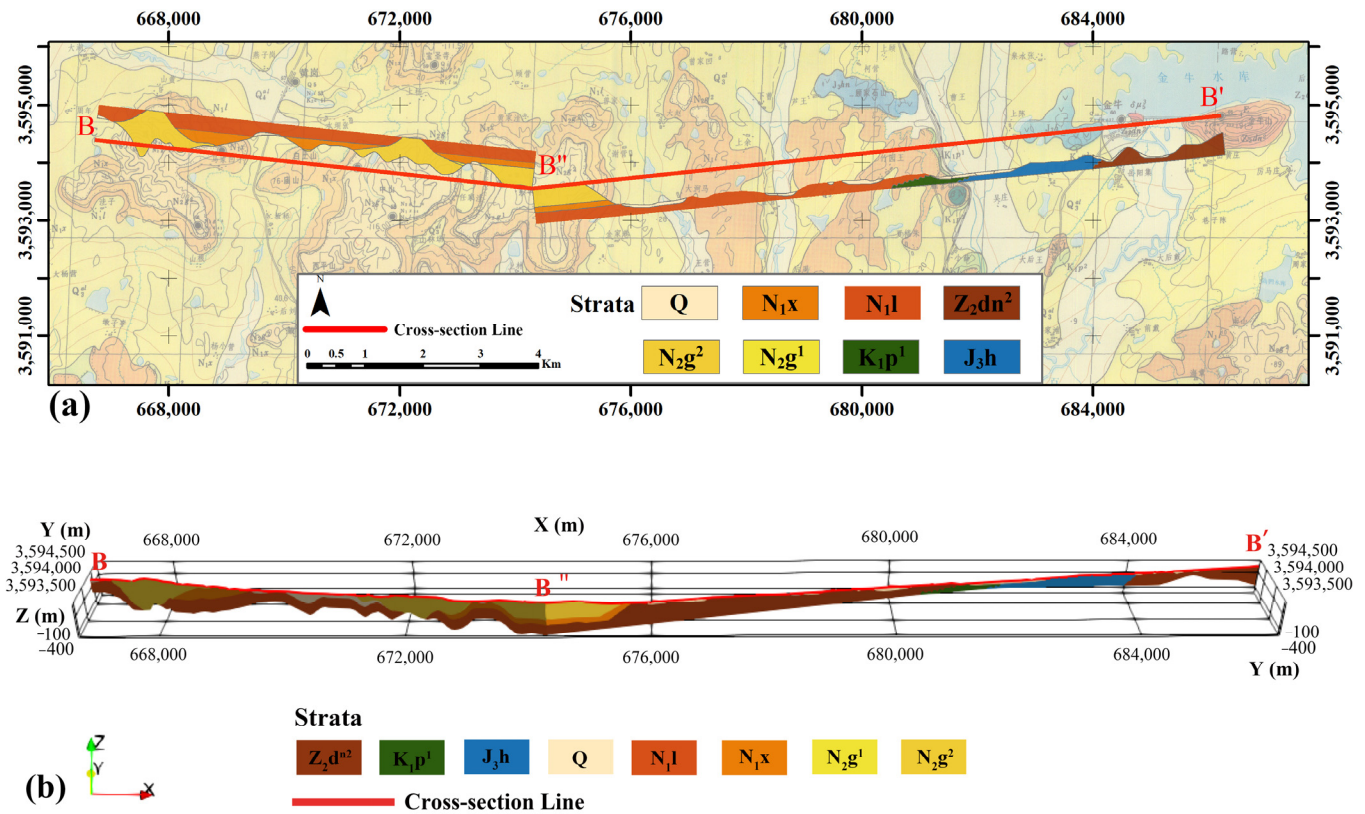


**Figure 6.** (a) The affine transformation effect of two branch GCs from the GC B-B''-B' divided into two parts at the turning point B''. In order to avoid overlap, this paper presents them in different directions. (b) The merged result after 3D transformation of the two branch GCs displayed with 3D coordinate axis.

### 3.5. Quantitative Tests of 3D Transformation Effect

To quantitatively evaluate the actual effect of all GCs after 3D transformation, two error values are proposed in this paper, i.e., NNG\_Error and NNC\_Error. NNG\_Error refers to the fitting error between the GC and the ground, which represents the fitting degree with the ground. The calculation process is as follows: first, sample points at a specific interval from the GL (the ground line in Section 3.4) of the 3D GC, record the number of sampling points as NNG, then calculate the absolute value of the difference between the elevation value of each sampling point and the DEM value at the location of the point, and finally, sum all absolute values and take the average value (Formula (4)). NNC\_Error refers to the deformation error of geometric nodes on the GC after the 3D transformation, representing the degree of geometric deformation of the GC. The calculation process is as follows: first, obtain all geometric nodes on the GC, recording the number as NNC, and calculate the two distance values, respectively. One is the vertical distance  $d_n$  between each geometric node  $P_s'$  after affine transformation to the GCL (SL in Section 3.2), and the other  $d_m$  is the absolute value of the difference between the elevation value  $z_s''$  of the geometric node  $P_s''$  and  $z_f'$  (the elevation value of the node  $P_f'$  in Section 3.3). Then, calculate the absolute value of the difference between the two distance values, and finally sum all the absolute values and take the average value (Formula (5)).

$$NNG\_Error = \frac{\sum_{i=1}^{NNG} |z_i - z_{DEM}|}{NNG} \tag{4}$$

where NNG is the number of sampling points,  $z_i$  is the elevation value of the sampling point, and  $z_{DEM}$  is the DEM value at the location of the point.

$$NNC\_Error = \frac{\sum_{i=1}^{NNC} |d_n - d_m|}{NNC} \quad (5)$$

where NNC is the number of geometric nodes on the GC,  $d_n$  is the vertical distance between each geometric node  $P_s'$  to the GCL (SL in Section 3.2), and  $d_m$  is the absolute value of the difference between the elevation value  $z_s''$  of the geometric node  $P_s''$  and  $z_f'$  (the elevation value of the node  $P_f'$  in Section 3.3).

#### 4. Experimental Results

The fourteen GCs in the study area are processed by the proposed method in Sections 3.1–3.4. The 3D transformed GCs are shown in Figure 7. Figure 7a is the global view, and Figure 7b–e is the local view.

From the global view shown in Figure 7a, it can be concluded that the 2D GCs completely match the actual location after being transformed into 3D GCs. Therefore, analyzing the distribution of 3D cross-sections in the study area will be more intuitive.

Figure 7b shows the scene where two 3D GCs intersect. It is clear to observe that the strata (e.g., Q, hb $\delta\mu^{21}$ ) at the intersection can be joined without dislocation. On the one hand, it is proved that the current DEM is consistent with the DEM when the two GCs are produced, and the ground undulation has not changed significantly. On the other hand, it is also well proved that the proposed method for transforming stratigraphic geometry is faithful and effective.

Figure 7c,d shows the fitting of the 3D GC and DEM from the upward view and the aerial view. When in the aerial view, set the DEM to a specific transparency for easy observation. The overall fitting effect is satisfactory, but some areas have slight deviations due to the small number of geometric nodes in the strata surfaces (the place indicated by the red arrow in Figure 7c).

Figure 7e shows the scene of the overlapping GC and planar geological map, which can easily and intuitively display the 3D distribution of strata. The planar geological map shows the distribution of strata in the horizontal direction, and the GC shows the distribution and depth in the vertical direction. The two work together to visualize the strata in 3D. For example, it is evident that the boundaries of the strata  $\lambda\pi^3$  and  $\tau\alpha\pi^{3y/5}$  in the cross-section could completely fit with these in the planar geological map. However, one point to note in this study area is the following: in the 2D GC, the Quaternary strata are not distinguished by age and are uniformly replaced by Q; the planar geological map distinguishes and gives different colors to the Quaternary strata of different ages, so the two will have color differences after fitting, but the result is correct.

According to the verification method provided in Section 3.5, this paper calculates the NNG\_Error and NNC\_Error of each GC in the study area (see Table 2). The NNG\_Error value ranges from 0.95 to 1.53 m, with a small error. Through analysis, the error mainly comes from the fact that the interval distance of some nodes on the original GC is greater than the DEM resolution. The NNC\_Error value ranges from 1.37–6.31 m, except for 13.48 m of GC B-B''-B'. The past terrain of GC B-B''-B' fluctuated considerably, and the current terrain is relatively flat, so the deformation degree of the stratum surface is apparent. The above data are within the acceptable range. On the one hand, it shows that the method in this paper is feasible for the 3D transformation of 2D GCs, and on the other hand, it proves that the current terrain of Nanjing has little change compared with the terrain in the 1970s–1990s.

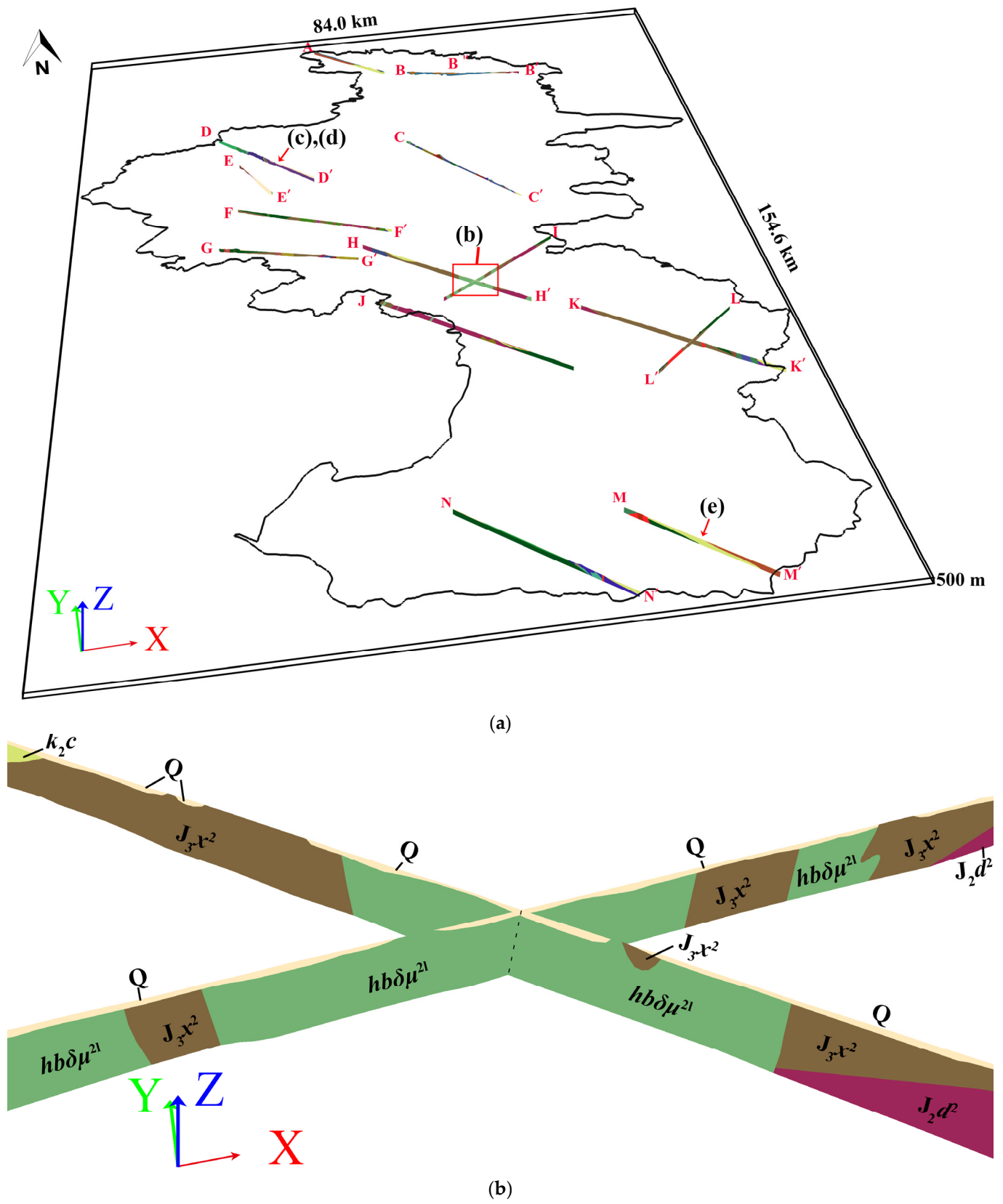
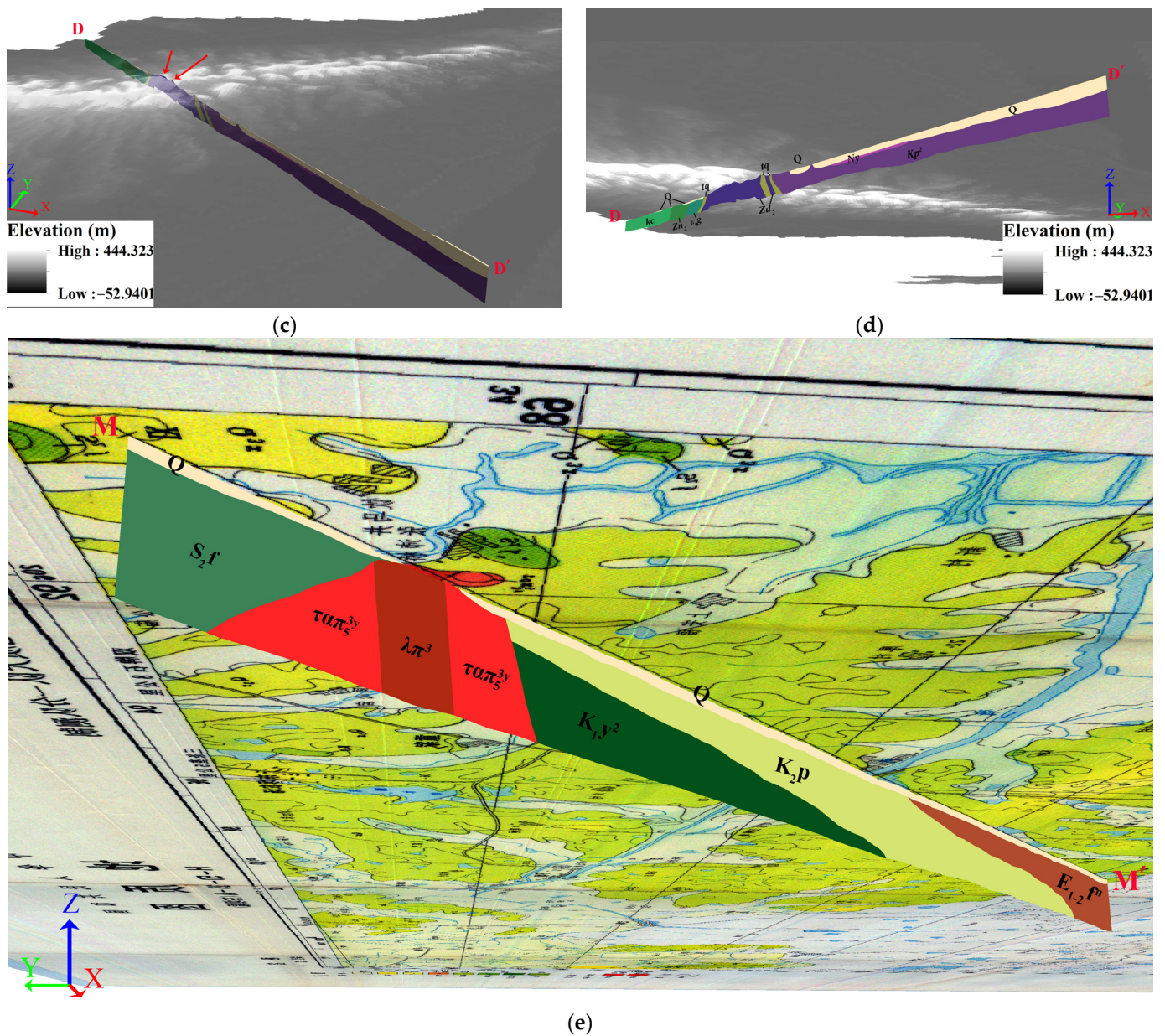


Figure 7. Cont.



**Figure 7.** Fourteen 3D GCs in Nanjing City. (a) The global view. (b) Intercross-section of two 3D GCs. (c,d) The 3D GC fits to the DEM. (e) The 3D GC fits to planar geological map. Note: In the 2D GC, the Quaternary strata are not distinguished by age and are uniformly replaced by Q. The planar geological map distinguishes and gives different colors to the Quaternary strata of different ages, so the two will have color differences after fitting.

**Table 2.** The fitting error and deformation error of each GC in the study area.

GC	A-A'	B-B''-B'	C-C'	D-D'	E-E'	F-F'	G-G'	H-H'	I-I'	J-J'	K-K'	L-L'	M-M'	N-N'
NNG	183	241	132	143	75	164	137	97	153	159	178	127	91	47
NNG_Error (m)	1.35	1.53	1.32	1.27	1.21	1.37	1.24	1.17	1.33	1.36	1.41	1.24	0.95	1.22
NNC	2411	3362	1347	1337	636	1823	1327	807	1626	1670	2130	1280	806	474
NNC_Error (m)	5.45	13.48	4.16	4.57	3.32	5.21	3.79	3.53	5.75	6.31	4.74	3.39	2.46	1.37

## 5. Discussion and Application

### 5.1. Factors Affecting the Method

#### 5.1.1. DEM at Different Periods

In Section 3.3, the elevation value is obtained from the DEM in the 3D transformation of each stratum surface, so the DEM is the most critical factor affecting the 3D transformation of the GCs in this paper. The DEM is made from actual surface absolute elevation data, a digital representation of surface morphology [38]. However, the ground elevation is dynamically changing due to the natural environment, geological environment, and human activities [39,40]. This means that the ground undulation corresponding to the GC constructed in the early period may be inconsistent with that obtained by the current DEM. In this study, each stratum surface in the GC being 3D transformed needs to use surface undulation to control the geometric shape fully. Therefore, when the difference in surface undulation in different periods is slight, the GC before and after transformation is consistent. On the contrary, when the difference is too significant, the geometric shape of the stratum surface in the transformed GC will be distorted, and the expression effect will be reduced. For the latter, conducting a geological field survey and even re-measuring the cross-section is often necessary. The elevation data obtained by satellite alone cannot be effectively processed.

#### 5.1.2. DEM Resolution and Number of Geometric Nodes in the GC

DEM resolution is an important index to reflect the fineness of surface morphology [41]. It is known that the higher the DEM resolution, the more detailed the expression of surface fluctuations, but the volume of data will increase geometrically. On the contrary, the low-resolution DEM expresses the surface morphology more roughly, and the local surface fluctuation cannot be effectively highlighted, but the data volume will be reduced. Many scientific researchers will select the most appropriate ones according to the influence of DEMs with different resolutions on the research results [42–44]. In recent years, advanced multi-resolution terrain models [45,46] can quickly store and organize DEM data of varying resolution levels in a specific area. They could meet the needs of 3D transformation of 2D GCs. Therefore, this paper suggests that geological workers obtain the multi-resolution terrain model in the experimental area and select the appropriate DEM resolution.

Each strata surface in the vector GC is composed of many geometric nodes. The number of nodes passing through the ground determines the surface undulation of the GC, thus affecting the accuracy of the 3D transformation result. Meanwhile, the coordinates of geometric nodes on the deep stratum surface are also controlled by the surface undulation, so the insufficient number of nodes will also change the original geometry of the stratum surface. When the resolution of the input DEM is fixed, if the distance between two adjacent nodes passing through the ground is greater than the resolution value, it is easy to cause the surface undulation on the GC and the ground undulation to fit incompletely. Moreover, for some GCs attached below the geological map, in the process of vectorization, due to the randomness of human editing, the number of nodes on the GC often cannot meet the requirements. In conclusion, if the above situations happen, the geometric nodes must be densified.

#### 5.1.3. Mapping Quality of GCs

No matter the automatic, semi-automatic, or manual GCs, there is much expert experience and different mapping requirements [47]. On the one hand, due to the difference in experts' experience and knowledge, the accuracy of GC mapping results will be affected. As the surveyed GCs are mapped mainly by a certain number of boreholes with expert knowledge inference, the number of boreholes, expert inference method, and other manual factors will affect the mapping error. Thus, in the process of the 3D transformation of the GCs, the error will be transferred and further expanded. For the surveyed GCs, it is necessary to invite experts or geological workers to assist in modification and then select the 3D transformation method proposed in this paper. On the other hand, most GCs will use the

same horizontal and vertical scales in the drawing process to ensure geometric authenticity. However, it is not ruled out that some geological work will expand the scale to reproduce the details of vertical or horizontal directions, resulting in geometric deformation [8]. Such GCs need to be transformed to the actual scale and then adopt the proposed method to obtain an accurate 3D result.

#### 5.1.4. Effects of Different 3D Transformation Strategies

Figure 5 shows that the geometric shape of GC M-M' after 3D transformation is constant compared with the original GC. On the contrary, Figure 6b shows that the geometric shape of GC B-B''-B' is significantly deformed. Through the analysis of the influencing factors, it can be seen that the main reason is the difference in the DEM in different periods. When the difference is slight, the effect of 3D transformation with the proposed method is better; otherwise, the effect is worse. In the process of 3D transformation of the GC, it is often a challenge to keep the geometric shape unchanged and ensure that it fits the actual terrain.

For the above reason, this study provides two other transformation strategies. One is to turn the GC 90 degrees to ensure that the geometric shapes remain unchanged before and after the transformation, called the Geometric Shape Maintenance Strategy [48]; the other is to determine the nodes' elevation value by subtracting the distance from the nodes to the surface from the ground elevation value, called the Surface Fitting Maintenance Strategy.

##### (1) Geometric Shape Maintenance Strategy

If the DEM constraint is not considered, the GC can be rotated 90 degrees counter-clockwise around the GCL SL. The following formula can be used to calculate the 3D coordinates of each node in the GC, which mainly includes five steps: translate to the origin, rotate  $\beta$  around the Z-axis, rotate  $\frac{\pi}{2}$  around the Y-axis, rotate  $2\pi - \beta$  around the Z-axis, and translate to the original position.

$$\begin{bmatrix} x_s'' \\ y_s'' \\ z_s'' \\ 1 \end{bmatrix} = \begin{bmatrix} 1 & 0 & 0 & x_f \\ 0 & 1 & 0 & y_f \\ 0 & 0 & 1 & 0 \\ 0 & 0 & 0 & 1 \end{bmatrix} \begin{bmatrix} \cos(2\pi - \beta) & -\sin(2\pi - \beta) & 0 & 0 \\ \sin(2\pi - \beta) & \cos(2\pi - \beta) & 0 & 0 \\ 0 & 0 & 1 & 0 \\ 0 & 0 & 0 & 1 \end{bmatrix} \begin{bmatrix} \cos(\frac{\pi}{2}) & 0 & \sin(\frac{\pi}{2}) & 0 \\ 0 & 1 & 0 & 0 \\ -\sin(\frac{\pi}{2}) & 0 & \cos(\frac{\pi}{2}) & 0 \\ 0 & 0 & 0 & 1 \end{bmatrix} \begin{bmatrix} \cos\beta & -\sin\beta & 0 & 0 \\ \sin\beta & \cos\beta & 0 & 0 \\ 0 & 0 & 1 & 0 \\ 0 & 0 & 0 & 1 \end{bmatrix} \begin{bmatrix} 1 & 0 & 0 & -x_f \\ 0 & 1 & 0 & -y_f \\ 0 & 0 & 1 & 0 \\ 0 & 0 & 0 & 1 \end{bmatrix} \begin{bmatrix} x_s' \\ y_s' \\ z_s' \\ 1 \end{bmatrix} \quad (6)$$

where  $\beta$  are the azimuths of the line SL;  $x_s'$ ,  $y_s'$ , and  $z_s'$  are the coordinates before the node is flipped;  $x_s''$ ,  $y_s''$ , and  $z_s''$  are the coordinates after the node is flipped; and  $x_f$  and  $y_f$  are the coordinates of the starting point  $P_f$  of the GCL SL.

##### (2) Surface Fitting Maintenance Strategy

The actual elevation value of node  $P_s'$  is obtained by subtracting the distance value  $d_3$  from node  $P_s'$  to point  $P_{GL}$  from the elevation value at point  $P_{SL}$ . Where  $x_s'' = x_{SL}$ ,  $y_s'' = y_{SL}$ . If node  $P_s'$  is located on the ground line GL, then  $z_s'' = z_{SL}$ ; otherwise,  $z_s'' = z_{SL} - d_3$ .

This paper still uses the GC B-B''-B' as the experimental case to show the result of the 3D transformation with two different strategies (Figure 8). By comparing the above two strategies (Figure 8a,b) with the proposed method (Figure 6b), we could observe the following facts: (1) The Geometric Shape Maintenance Strategy can maintain the geometry

of the GC, but it cannot closely fit the surface. The Surface Fitting Maintenance Strategy is greatly affected by surface undulation, so the geometric deformation is relatively severe. The proposed method is integrated between the two, and the transformed effect is improved. (2) Theoretically, when the actual surface undulation is consistent with the GC surface undulation, the three strategies can obtain a consistent 3D GC. When the gap between the two is small, the proposed method is better than the Surface Fitting Maintenance Strategy, but the time complexity is increased. When the gap is wide, specific strategies should be considered according to the different situations.

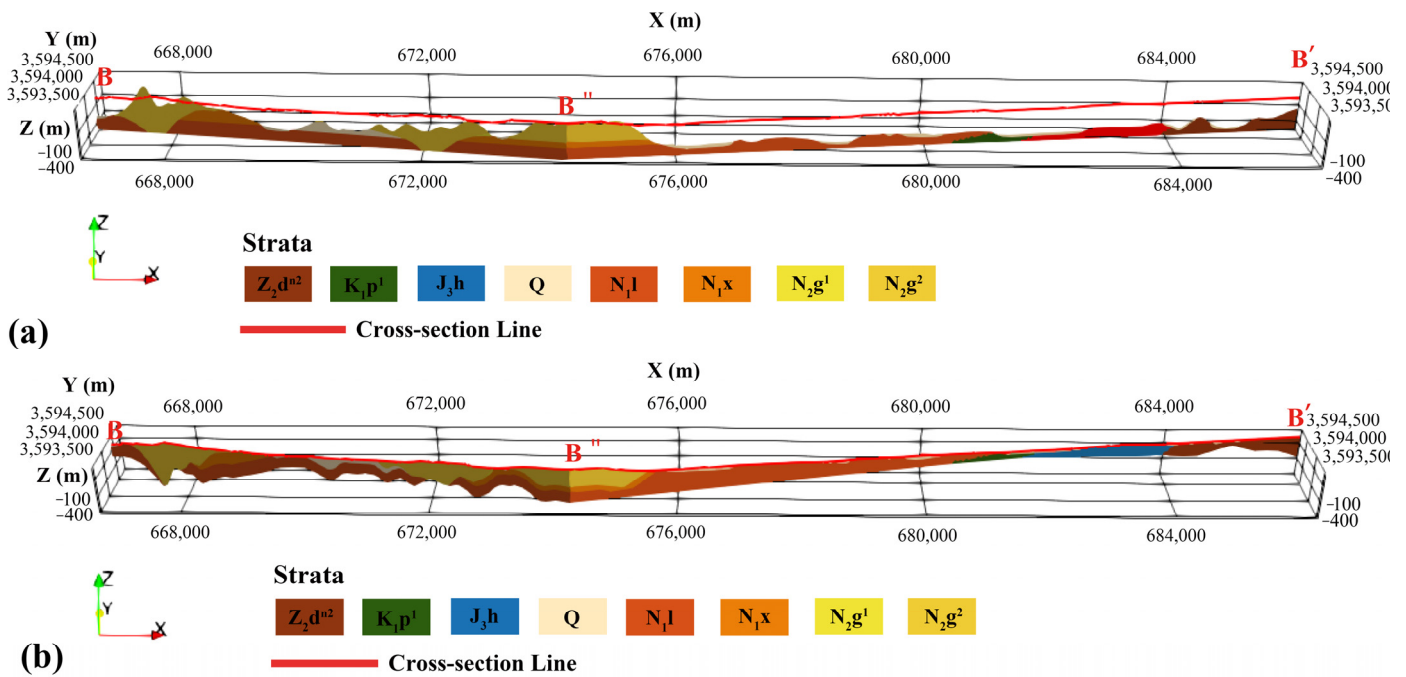


**Figure 8.** Two other 3D transformation strategies are applied to transform the GC B-B''-B': (a) Geometric Shape Maintenance Strategy. (b) Surface Fitting Maintenance Strategy. The transformed results are displayed with 3D coordinate axis.

5.2. Applicability of the Method

The mapping principle of geological cross-sections is the crucial factor in determining whether they can use the proposed method in this paper for 3D transformation. Due to the differences in geological mapping departments, mapping strategies, mapping methods, and other mapping factors, the expression forms of geological cross-sections are various. This proposed method applies to many types of geological cross-sections, but proper pre-treatment is required in the following cases:

- (1) The boundary lines on the left and right sides of the geological cross-section are not vertical. It is an essential prerequisite for the proposed method that the boundary lines on both sides are vertical. With non-vertical lines, it is difficult to effectively match corresponding points and generate feature lines, which affects the accuracy of the 3D transformation;
- (2) Vertical or horizontal exaggeration. General geological cross-sections will be mapped with the same vertical and horizontal scales (true-scale cross-sections) [8]. When constructing large regional or semi-regional cross-sections. Typically, it is the vertical scale that is exaggerated. This kind of geological cross-section needs to be transformed to the actual scale and then adopts the proposed method to obtain an accurate result.

### 5.3. Application Cases of the Transformed 3D GCs

#### 5.3.1. 3D Geological Modeling

The 3D geological model is an essential research object in geological research, underground engineering design, and other fields [49–51], and the GC is an important data source for 3D geological modeling. Multiple 2D GCs whose GCLs are parallel transformed into 3D GCLs can be used to build the 3D geological model by contour algorithm [26–28], morphing algorithm [29], or discrete smooth interpolation (DSI) algorithm [30]. The contour algorithm is the most mature.

There are no multiple parallel and close GCs in the study area of this paper, resulting in the inability to build local 3D models of the geological bodies. However, a single GC is almost consistent with the parallel GC at a certain distance on both sides in stratigraphic information and geometric shape [52]. Therefore, we could construct an additional GC that is the same and parallel to the original 3D GC and then construct a local 3D geological model based on the contour algorithm. Taking each stratum within the GC as the modeling unit, the 3D modeling process is as follows: first of all, translate each 3D stratum surface  $s_o''$  along the direction perpendicular to the GCL according to the strip distance  $\omega$  to obtain the parallel stratum surface  $s_o'''$ ; then, reconstruct the side between the two strata surfaces using the shortest distance method in the contour algorithm; and finally, close all geometric surfaces to construct the stratigraphic 3D solid model. The bent GC can be split into several straight GCs, each modeled as a 3D solid using the above-mentioned method and subsequently merged into a whole. Figure 9 shows the 3D solid models of GCs M-M' and B-B''-B'.

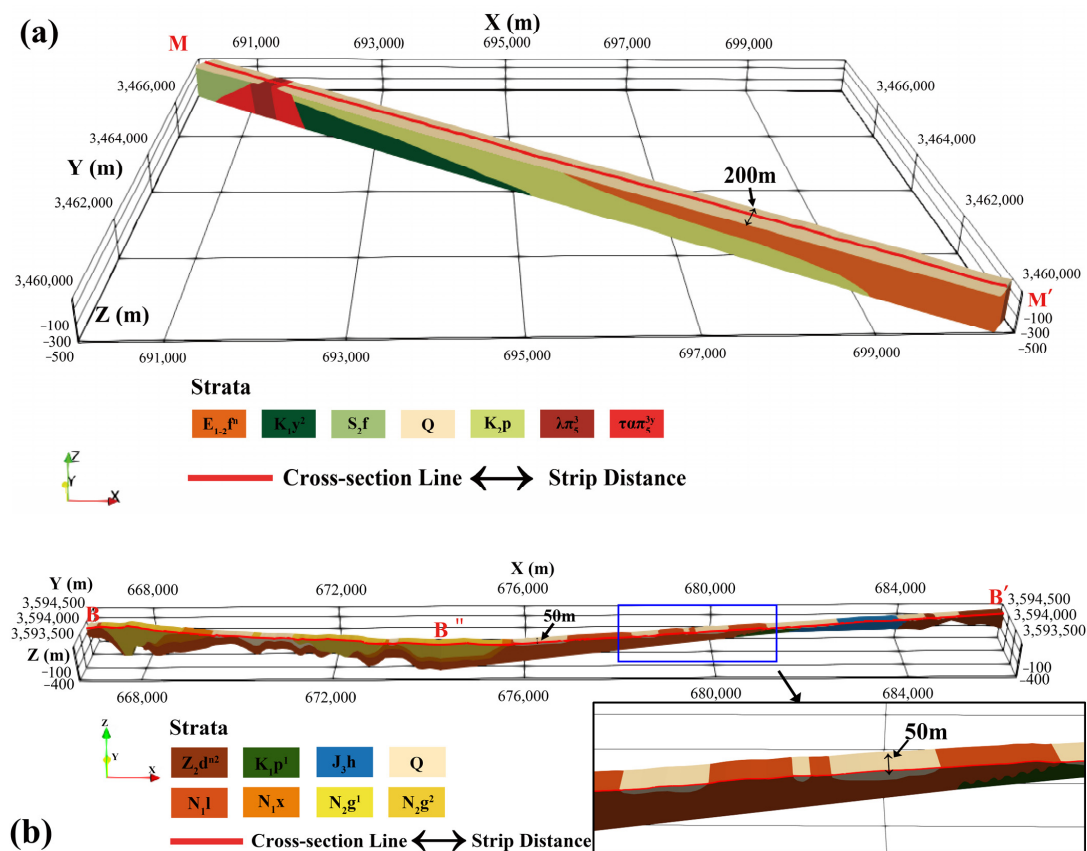


**Figure 9.** The 3D solid models constructed with two parallel 3D GCs and displayed with 3D coordinate axis. (a) 3D solid model of the GC M-M'. The strip distance is 200 m, 100 m on both side. (b) 3D solid model of the GC B-B''-B'. The strip distance is 50 m and the lower right corner is a partial enlarged view.

The strip distance  $\omega$  is the crucial factor in determining whether the 3D modeling of a single GC is effective. The value of  $\omega$  depends on the geological environment in the study area. The distance value should be as small as possible for areas with intense tectonic activity. On the contrary, the distance value can be further increased for a stable sedimentary environment area. It is also acceptable for some unturned fold zones when the distance between the parallel cross-sections is far [7]. Of course, the corresponding distances of different GCs in the same area are also different. Therefore, by comparing the 14 GCs and their geological maps in Nanjing, we selected different strip distances to build their 3D solid models (Figure 10).

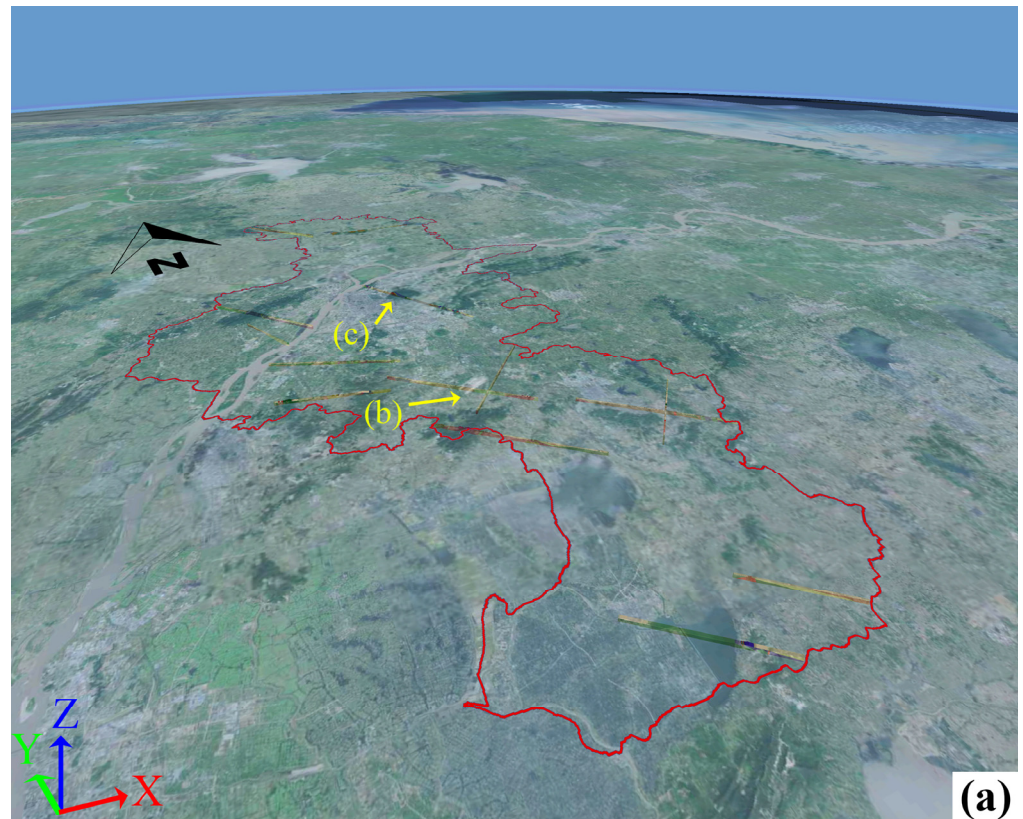


Figure 10. Cont.

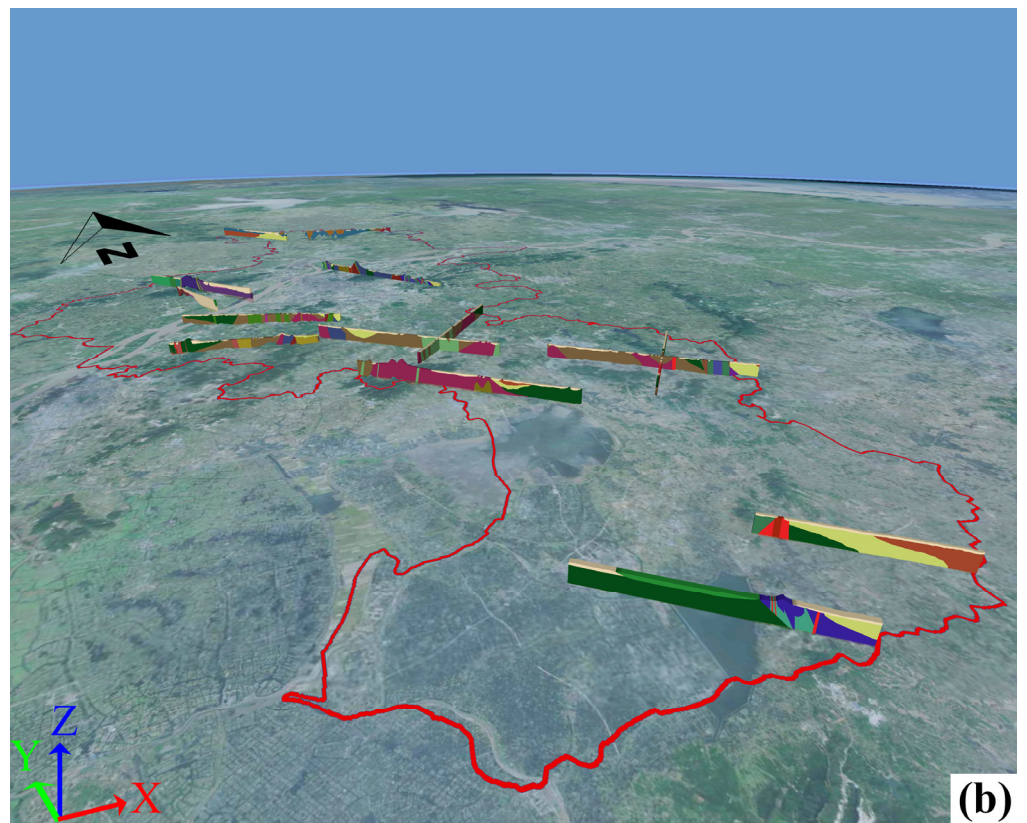
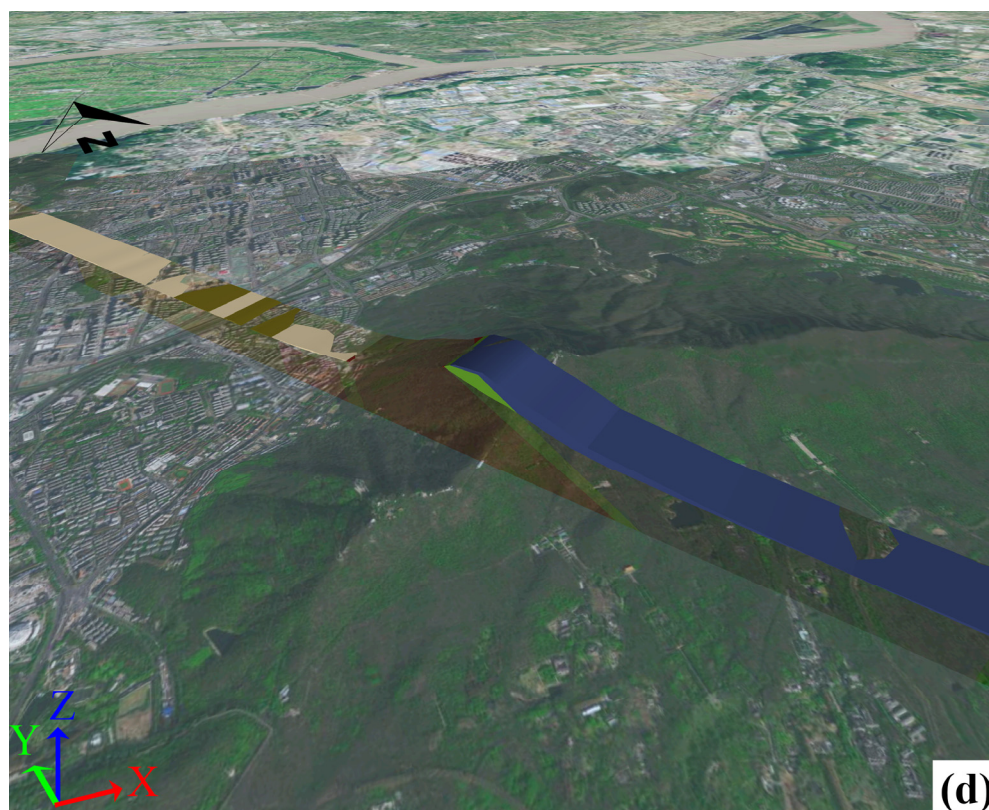


Figure 10. Cont.



**Figure 10.** (a) The 3D presentation effect of fourteen 3D models of all GCs in Nanjing City on Google Earth. (b) For convenient observation, we exaggerated the Z-axis of all 3D models by three times the elevation and moved it up to the ground. (c) The local looking-up view for observing the intersection of two 3D models. (d) The local looking-down view for observing the fitting of the 3D model with the ground.

### 5.3.2. 3D Presentation on the Digital Earth

It is significant to display the 3D transformed GCs in a 3D natural environment. On the one hand, it can express the degree of fit with the real world. On the other hand, it can show the development trend of the underground rock strata and assist geological surveys and underground engineering. This paper constructed the transformed GCs into 3D solid models (ESRI Shapefile format) to display the 3D shape in Google Earth. Figure 10a,b uses two different rules to show the effect of 3D geological solids in the actual scene. The former does not process the 3D geological models and observes their position by setting transparency on the image. The latter exaggerates the Z-axis of the 3D geological solids by three times and moves it up to the ground to clearly observe the distribution of the strata. Figure 10c,d are two local views. The former observes the combination effect of the intersection position of the two 3D models by looking up, and the latter observes the fit effect of the 3D model with the ground by looking down. We can observe that the 3D geological models can fit well with the surface and we can clearly observe the trend and distribution of the underground strata. In addition, the 3D cross-section or 3D solid models generated in this paper can be converted into OBJ, FBX, and other 3D formats and can therefore be displayed in Cesium, Skyline Globe, and other digital Earth platforms.

### 5.3.3. Parameter Setting of 3D Geological Models of GCs Display Effect

The 3D geological models' display effect is affected by the area's size and the observation angle, so they generally need to be adjusted by exaggerating the model or placing the position. Through multiple tests, this paper obtains the following schemes that best display the actual effect of the 3D geological models of GCs: (1) when in global view and

looking down, the 3D models can be exaggerated in the Z-axis and moved up to the ground (Figure 10b); (2) when in global view and looking up, the 3D models can be exaggerated in the Z-axis and not be shifted (Figure 11a); (3) when in local view and looking down, the 3D geological model can be moved up to the surface (Figure 11b) or the transparency of the image can be set (Figure 10d); (4) when in local view and looking up, we could adjust the position and angle of looking up to obtain the best impression (Figure 10c,d).

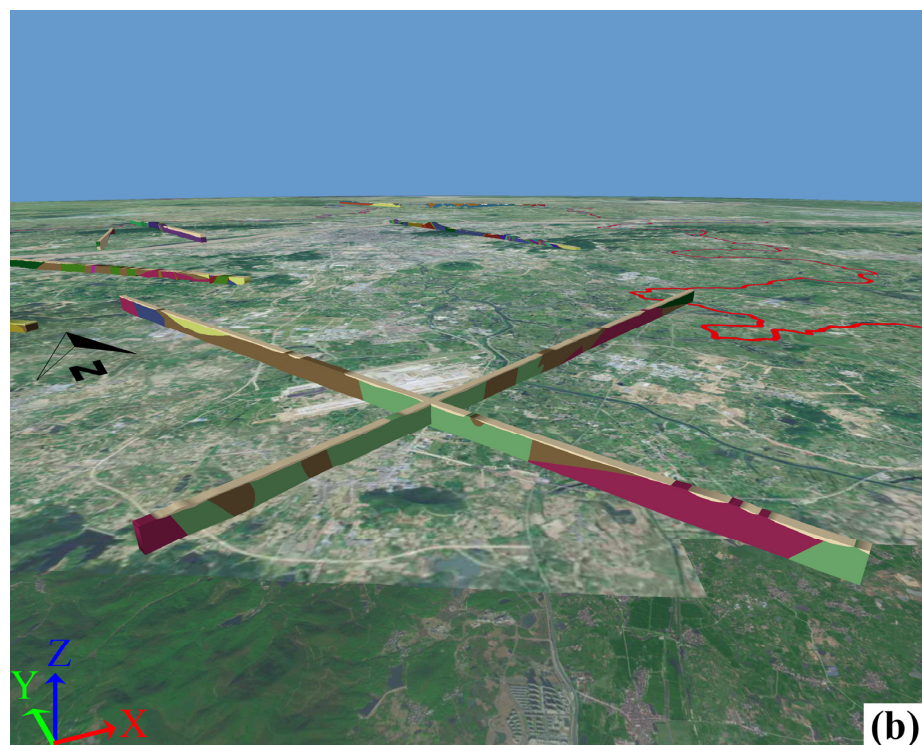
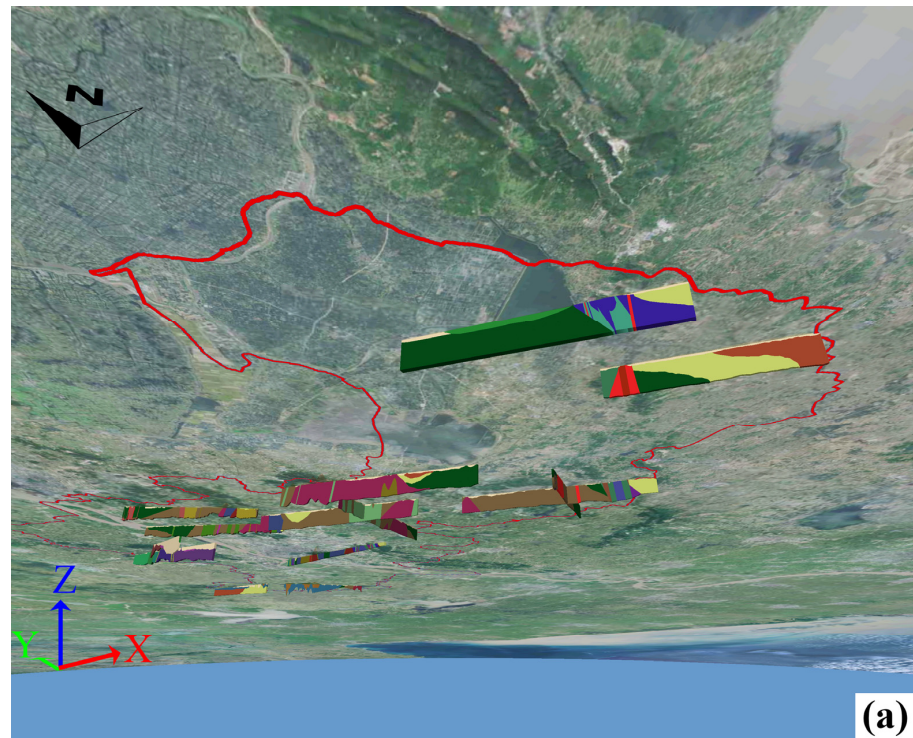
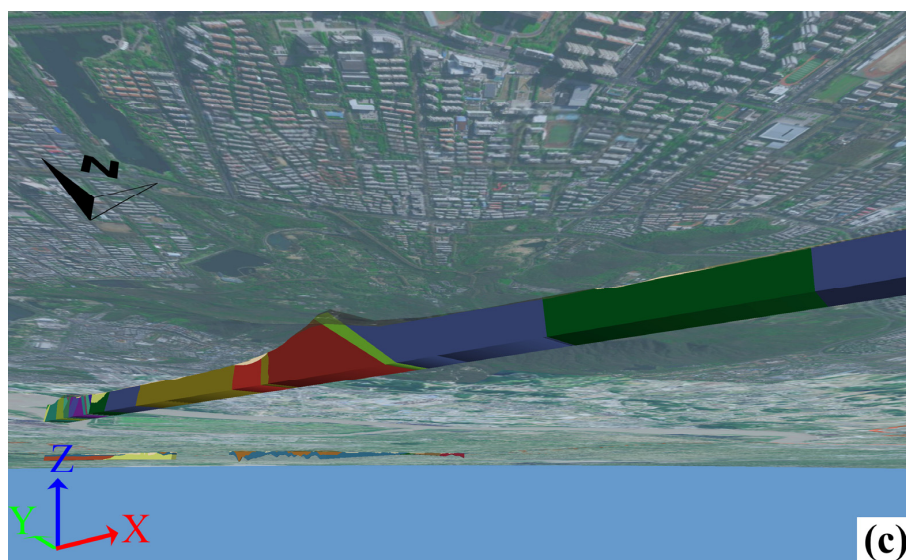


Figure 11. Cont.



**Figure 11.** Take the three scenarios in Figure 10a–d as examples to show the optimal observation scheme in different regions and different perspectives. (a) When looking up in the global view, the Z-axis exaggeration can be more intuitive. (b) When looking down in the local view, the 3D geological model can be moved up to observe the stratigraphic geometric shape and distribution. (c) When looking up in the local view, the best display effect can be achieved by rotating the viewing positions and angles.

## 6. Conclusions

This paper discussed an automatic generation method of 3D GCs by increasing the dimensions to expand the application scenarios of 2D GCs and meet the application requirements of 3D geology. The proposed method first used geometric affine transformation and GIS technology to realize the constraint of the GCL and DEM on the geometric shape or undulation of each stratum surface. Then, it designed different equations for calculating the elevation value of each node by classifying all nodes. Finally, all 3D strata surfaces are merged into a 3D GC. This paper transformed fourteen 2D GCs into 3D GCs in Nanjing City, Jiangsu Province. The experimental results showed that the proposed method had a good effect on the processing strategy of straight and bent GCs, the control of the geometric shape of GCs, and the realization of a seamless fit with the ground.

This paper explored the different factors that affect the effect of 3D transformation and put forward solutions for, or opinions on, solving related problems to assist geological decision-making. By comparing three different 3D transformation strategies, the advantages of the proposed method are verified laterally. As far as the application is concerned, the generated 3D GCs can be used for 3D geological modeling and the 3D reality display of the digital Earth to meet the needs of actual geological engineering and scientific expression. In addition, for the scene display of the 3D GC models, we proposed different optimization schemes for geologists to reference and select.

**Author Contributions:** Hao Shang conceived the original idea and is the primary author of the manuscript. Yan-Gen Shen and An-Bo Li developed the main modules of the prototype system and are the key contributors to the methodology. Shuang Li developed partial modules of the prototype system. Tao Zhang processed relative data. All authors have read and agreed to the published version of the manuscript.

**Funding:** This study was supported by the National Key R&D Program of China (No. 2022YFB3904104) and by the National Natural Science Foundation of China (Project No. 41971068, 41771431).

**Institutional Review Board Statement:** Not applicable.

**Informed Consent Statement:** Not applicable.

**Data Availability Statement:** Not applicable.

**Conflicts of Interest:** The authors declare no conflict of interest.

## References

- Ragan, D.M. Maps and Cross Sections. In *Structural Geology: An Introduction to Geometrical Techniques*; Cambridge University Press: New York, NY, USA, 2009; p. 518.
- Brozzetti, F.; Boncio, P.; Cirillo, D.; Ferrarini, F.; De Nardis, R.; Testa, A.; Liberi, F.; Lavecchia, G. High-Resolution Field Mapping and Analysis of the August–October 2016 Coseismic Surface Faulting (Central Italy Earthquakes): Slip Distribution, Parameterization, and Comparison with Global Earthquakes. *Tectonics* **2019**, *38*, 417–439. [[CrossRef](#)]
- Pierantoni, P.; Deiana, G.; Galdenzi, S. Stratigraphic and Structural Features of the Sibillini Mountains (Umbria-Marche Apennines, Italy). *Ital. J. Geosci.* **2013**, *132*, 497–520. [[CrossRef](#)]
- Birch, G.F.; Lound, S.P.; Goodwin, I.D. The Late Quaternary Geological History of the Upper and Central Sydney Estuary (Australia). *Reg. Stud. Mar. Sci.* **2022**, *53*, 102394. [[CrossRef](#)]
- Saini, D.P.; Mukhopadhyay, D.K.; Mishra, P. Balanced Cross Sections and Kinematic Evolution Across Digboi Oil Field, Northeast India. *J. Geol. Soc. India* **2022**, *98*, 487–495. [[CrossRef](#)]
- Wang, Y.; Shi, C.; Li, X. Machine Learning of Geological Details from Borehole Logs for Development of High-Resolution Subsurface Geological Cross-Section and Geotechnical Analysis. *Georisk* **2022**, *16*, 2–20. [[CrossRef](#)]
- Hao, M.; Li, M.; Zhang, J.; Liu, Y.; Huang, C.; Zhou, F. Research on 3D Geological Modeling Method Based on Multiple Constraints. *Earth Sci. Inform.* **2021**, *14*, 291–297. [[CrossRef](#)]
- Tearpock, D.J.; Bischke, R.E. Cross Sections. In *Applied Subsurface Geological Mapping with Structural Methods*; Prentice Hall: Hoboken, NJ, USA, 2002; p. 175.
- Kubac, J.; Marschalko, M.; Niemiec, D.; Yilmaz, I.; Cheng, X.; Duraj, M. Quantification of the Quaternary Geological Structure Using Geological Cross-Sections in a Selected Part of the Moravian-Silesian Region for Geotechnical Purposes. In *IOP Conference Series: Materials Science and Engineering*; IOP Publishing: Bristol, UK, 2019; Volume 471, p. 042005.
- Zhang, Z.; Wu, C.; Mao, X.; Yao, W. Method and Technique of 3-D Dynamic Structural Evolution Modelling of Fault Basin. *Int. J. Oil Gas Coal Technol.* **2013**, *6*, 40–62. [[CrossRef](#)]
- Li, A.; Zhou, L.; Lv, G. Geological Information System. In *Geological Information System*; China Science Publishing & Media Ltd.: Beijing, China, 2013; pp. 76–93.
- Maltman, A. Geological Cross-Sections. In *Geological Maps: An Introduction*; Springer Science & Business Media: New York, NY, USA, 2012; pp. 52–60, ISBN 978-0-442-30307-5.
- Li, L.; Chen, K.; Yu, J.; Wang, J.; Luo, H. Parametric modelling of the Geological cross section for shield tunnel design and construction. *ISPRS Ann. Photogramm. Remote Sens. Spat. Inf. Sci.* **2022**, *10*, 177–184. [[CrossRef](#)]
- Guo, J.; Zhang, R.; Wu, L.; Yang, Y. An Automatic Method for Generating Curvilinear Geological Section with Stratal Pinch-Out. In Proceedings of the 2011 IEEE International Geoscience and Remote Sensing Symposium, Vancouver, BC, Canada, 24–29 July 2011; IEEE: Piscataway, NJ, USA, 2011; pp. 2965–2968.
- Shen, Y.-G.; Li, A.-B.; Huang, J.-C.; Lü, G.-N.; Li, K.-L. Three-Dimensional Modeling of Loose Layers Based on Stratum Development Law. *Open Geosci.* **2022**, *14*, 1480–1500. [[CrossRef](#)]
- Hassanzadeh, A.; Vázquez-Suñé, E.; Corbella, M.; Criollo, R. An Automatic Geological 3D Cross-Section Generator: Geopropy, an Open-Source Library. *Environ. Model. Softw.* **2022**, *149*, 105309. [[CrossRef](#)]
- Wu, X.; Liu, G.; Weng, Z.; Tian, Y.; Zhang, Z.; Li, Y.; Chen, G. Constructing 3D Geological Models Based on Large-Scale Geological Maps. *Open Geosci.* **2021**, *13*, 851–866. [[CrossRef](#)]
- Ran, X.; Xue, L.; Sang, X.; Pei, Y.; Zhang, Y. Intelligent Generation of Cross Sections Using a Conditional Generative Adversarial Network and Application to Regional 3D Geological Modeling. *Mathematics* **2022**, *10*, 4677. [[CrossRef](#)]
- Levorsen, A.I. *Paleogeologic Maps*; W. H. Freeman and Company: San Francisco, CA, USA, 1960.
- Lobeck, A.K. *Block Diagrams and Other Graphic Methods Used in Geology and Geography*, 2nd ed.; Emerson-Trussell Book Company: Amherst, MA, USA, 1958.
- Wu, Q.; Xu, H.; Zou, X. An Effective Method for 3D Geological Modeling with Multi-Source Data Integration. *Comput. Geosci.* **2005**, *31*, 35–43. [[CrossRef](#)]
- Lin, B.; Zhou, L.; Lv, G.; Zhu, A. 3D Geological Modelling Based on 2D Geological Map. *Ann. GIS* **2017**, *23*, 117–129. [[CrossRef](#)]
- Wang, L.; Yin, Y.; Wang, H.; Zhang, C.; Feng, W.; Liu, Z.; Wang, P.; Cheng, L.; Liu, J. A Method of Reconstructing 3D Model from 2D Geological Cross-Section Based on Self-Adaptive Spatial Sampling: A Case Study of Cretaceous McMurray Reservoirs in a Block of Canada. *Pet. Explor. Dev.* **2021**, *48*, 407–420. [[CrossRef](#)]
- Zhuang, C.; Zhu, H.; Wang, W.; Liu, B.; Ma, Y.; Guo, J.; Liu, C.; Zhang, H.; Liu, F.; Cui, L. Research on Urban 3D Geological Modeling Based on Multi-Modal Data Fusion: A Case Study in Jinan, China. *Earth Sci. Inform.* **2022**, *16*, 549–563. [[CrossRef](#)]
- Chen, Q.; Mariethoz, G.; Liu, G.; Comunian, A.; Ma, X. Locality-Based 3-D Multiple-Point Statistics Reconstruction Using 2-D Geological Cross Sections. *Hydrol. Earth Syst. Sci.* **2018**, *22*, 6547–6566. [[CrossRef](#)]
- Keppel, E. Approximating Complex Surfaces by Triangulation of Contour Lines. *IBM J. Res. Dev.* **1975**, *19*, 2–11. [[CrossRef](#)]

27. Ekoule, A.B.; Peyrin, F.C.; Odet, C.L. A Triangulation Algorithm from Arbitrary Shaped Multiple Planar Contours. *ACM Trans. Graph.* **1991**, *10*, 182–199. [[CrossRef](#)]
28. Ganapathy, S.; Dennehy, T.G. A New General Triangulation Method for Planar Contours. *ACM Siggraph Comput. Graph.* **1982**, *16*, 69–75. [[CrossRef](#)]
29. Ming, J.; Yan, M. Three-Dimensional Geological Surface Creation Based on Morphing. *Geogr. Geo-Inf. Sci.* **2014**, *30*, 37–40. (In Chinese) [[CrossRef](#)]
30. Frank, T.; Tertois, A.-L.; Mallet, J.-L. 3D-Reconstruction of Complex Geological Interfaces from Irregularly Distributed and Noisy Point Data. *Comput. Geosci.* **2007**, *33*, 932–943. [[CrossRef](#)]
31. Xie, Z. Stratigraphy. In *Memoir on Geology of Nanjing-Zhengjiang Mountains*; Phoenix Publishing & Media. Inc.: Nanjing, China, 1989; pp. 6–12.
32. Nomizu, K.; Katsumi, N.; Sasaki, T. *Affine Differential Geometry: Geometry of Affine Immersions*, 1st ed.; Cambridge University Press: London, UK, 1994.
33. Brannan, D.A.; Esplen, M.F.; Gray, J.J. *Affine Geometry*. In *Geometry*; Cambridge University Press: London, UK, 2011; pp. 61–84.
34. Song, Z.; Zhou, S.; Guan, J. A Novel Image Registration Algorithm for Remote Sensing under Affine Transformation. *IEEE Trans. Geosci. Remote Sens.* **2013**, *52*, 4895–4912. [[CrossRef](#)]
35. Hafez, A.Z.; Soliman, A.; El-Metwally, K.A.; Ismail, I.M. Tilt and Azimuth Angles in Solar Energy Applications—A Review. *Renew. Sustain. Energy Rev.* **2017**, *77*, 147–168. [[CrossRef](#)]
36. Vanicek, P.; Krakivsky, E.J. Applications of Geodesy. In *Geodesy: The Concepts*; Elsevier Science: New York, NY, USA, 2015; p. 19.
37. Cohen, D.; Lee, T.B.; Sklar, D. A Problems-Oriented Approach. In *Precalculus*; Cengage Learning: Boston, MA, USA, 2016; p. 698.
38. Miller, C.L. The Theory and Application of the Digital Terrain Model. Ph.D. Thesis, Massachusetts Institute of Technology, Cambridge, MA, USA, 1958.
39. Evans, I.S. Geomorphometry and Landform Mapping: What Is a Landform? *Geomorphology* **2012**, *137*, 94–106. [[CrossRef](#)]
40. Lizarazo, I.; Angulo, V.; Rodríguez, J. Automatic Mapping of Land Surface Elevation Changes from UAV-Based Imagery. *Int. J. Remote Sens.* **2017**, *38*, 2603–2622. [[CrossRef](#)]
41. Maune, D.F.; Nayegandhi, A. Quality Assessment of Elevation Data. In *Digital Elevation Model Technologies and Applications-The DEM Users Manual*; Asprs Pubns: Baton Rouge, Louisiana, 2009; pp. 450–455.
42. Schoorl, J.M.; Sonneveld, M.P.W.; Veldkamp, A. Three-dimensional landscape process modelling: The effect of DEM resolution. *Earth Surf. Process. Landf.* **2000**, *25*, 1025–1034. [[CrossRef](#)]
43. Sørensen, R.; Seibert, J. Effects of DEM Resolution on the Calculation of Topographical Indices: TWI and Its Components. *J. Hydrol.* **2007**, *347*, 79–89. [[CrossRef](#)]
44. Thompson, J.A.; Bell, J.C.; Butler, C.A. Digital Elevation Model Resolution: Effects on Terrain Attribute Calculation and Quantitative Soil-Landscape Modeling. *Geoderma* **2001**, *100*, 67–89. [[CrossRef](#)]
45. Brůha, L.; Kolář, J. A Procedural Footprint Enhancement of Global Topographic Surface with Multiple Levels of Detail. *Int. J. Digit. Earth* **2020**, *13*, 527–545. [[CrossRef](#)]
46. Zhai, R.; Lu, K.; Pan, W.; Dai, S. GPU-Based Real-Time Terrain Rendering: Design and Implementation. *Neurocomputing* **2016**, *171*, 1–8. [[CrossRef](#)]
47. Bose, N.; Mukherjee, S. *Map Interpretation for Structural Geologists*, 1st ed.; Elsevier: Cambridge, UK, 2017.
48. Walsh, G.J. A Method for Creating a Three Dimensional Model from Published Geologic Maps and Cross Sections. *US Geol. Surv. Open-File Rep.* **2009**, *1229*, 16. [[CrossRef](#)]
49. Schweizer, D.; Blum, P.; Butscher, C. Uncertainty Assessment in 3-D Geological Models of Increasing Complexity. *Solid Earth* **2017**, *8*, 515–530. [[CrossRef](#)]
50. Wycisk, P.; Hubert, T.; Gossel, W.; Neumann, C. High-Resolution 3D Spatial Modelling of Complex Geological Structures for an Environmental Risk Assessment of Abundant Mining and Industrial Megasites. *Comput. Geosci.* **2009**, *35*, 165–182. [[CrossRef](#)]
51. Li, A.-B.; Chen, H.; Du, X.-F.; Sun, G.-K.; Liu, X.-Y. Parametric Modeling Method for 3D Symbols of Fold Structures. *ISPRS Int. J. Geo-Inf.* **2022**, *11*, 618. [[CrossRef](#)]
52. Boggs, S. Depositional Environments. In *Principles of Sedimentology and Stratigraphy*; Prentice Hall Boston: Boston, MA, USA, 2012; p. 209.

**Disclaimer/Publisher’s Note:** The statements, opinions and data contained in all publications are solely those of the individual author(s) and contributor(s) and not of MDPI and/or the editor(s). MDPI and/or the editor(s) disclaim responsibility for any injury to people or property resulting from any ideas, methods, instructions or products referred to in the content.